Multimodal-TERESA, a ^{210}Pb-based radiometric dating model for recent sediments under largely varying rates of supply

J.M. Abril Hernández

Dpto. Física Aplicada I, ETSIA Universidad de Sevilla, Sevilla (Spain), Carretera de Utrera km 1, D.P. 41013, Seville, Spain

Keywords:

^{210}Pb dating
Recent sediments
Varying fluxes
Model errors
Multimodal distributions
TERESA model

A B S T R A C T

Lead-210 from natural atmospheric fallout is widely used in multidisciplinary studies for dating recent sedi-ments. In anthropogenically-impacted and/or high energy systems the ^{210}Pb flux onto the sediments may show non-random temporal variability, leading to the failure of classical dating models. The problem of how identi-fying and dating such cases remained unsolved, and it is the goal of the present work. Empirical evidences from varved sediments prove that initial activity concentrations of excess ^{210}Pb (^{210}Pb$_{exc}$) and sediment accumulation rates (SARs) show large and independent temporal variability. M-TERESA model describes such variability by using multimodal frequency distributions and decodes the chronology from the ^{210}Pb$_{exc}$ versus mass depth profile. The new model can solve scenarios with largely varying rates of supply, which fall beyond the limits of the piecewise versions of the classical models. Its use is demonstrated with some complex ^{210}Pb$_{exc}$ profiles from varved sediments and synthetic cores for which an alternative and complete reconstruction of palaeofluxes and SARs is possible. The paper is supported by a wide set of supplementary material, including numerical codes for applying TERESA. The proposed methods are also useful for improving the reliability of routinely applications of the ^{210}Pb-based radiometric dating of recent sediments.

1. Introduction

The study of ^{210}Pb found in excess (^{210}Pb$_{exc}$ hereafter) with respect to its parent radionuclide (^{226}Ra) in sediment cores has shown to provide useful insights on the functioning of the sedimentary systems at a centennial time scale (Carroll and Lerche, 2003; Mabit et al., 2014). The ^{210}Pb dating method relies on the particular cycle of this radionuclide in nature (Robbins, 1978). The ^{222}Rn exhaled from the earth's surface into the free atmosphere is rapidly dispersed and diluted, and it decays to ^{210}Pb, which is removed by precipitation and dry deposition. This fallout ^{210}Pb can reach the surficial sediments, where it superposes to the ^{210}Pb produced by the in situ decay of ^{222}Rn (assumed in secular equilibrium with ^{226}Ra). In the buried sediments the ^{210}Pb$_{exc}$ signal decays with a known half-life (22.3 y), allowing for the construction of an internal clock. This method has become a widely used tool for multidisciplinary research, with about 5400 published documents (SCOPUS, "sediment" AND "^{210}Pb").

The revisited diagenetic equations (Abril, 2003) provide the physical fundamentals for the mass-conservation of a particle-bound radioactive tracer in porous and accreting sediments. Nevertheless, a chronology cannot be inferred from a ^{210}Pb$_{exc}$ versus depth profile without the set of assumptions which conforms a dating model. Different dating models are linked to the natural diversity in boundary and within-system conditions, which may involve mass and radionuclide fluxes onto the sediment-water interface (SWI) being constant or varying over time, being ideally deposited over the previously existing material or being depth-distributed, and with or without post-depositional redistributions. A summary of the most known ^{210}Pb-based dating models can be found in Mabit et al. (2014). As a brief update of the above review it is worth mentioning the critical revision of the physical fundamentals of the SIT model (Abril, 2015), the new TERESA model (Abril, 2016), and the Bayesian formulation of the "constant rate of supply" (CRS) model, by Aquino-López et al. (2018).

Although non ideal deposition and post-depositional redistribution have been widely described and modelled (e.g., Abril and Gharbi, 2012; Christensen, 1982; Robbins and Edgington, 1975) they seem to be important only in a minority of the published studies. The set of models considered in this work share three assumptions: i) continuity of the sequence (i.e., there is not any missing layer by erosion, neither huge episodic depositional-events); ii) ^{210}Pb$_{exc}$ behaves as a particle-associated tracer and new inputs are ideally deposited onto the SWI; iii) there is no post-depositional redistribution. An additional

E-mail address: jmabril@us.es.

Table 1
Performance tests for the CF-CS model under temporal variability in SAR and initial activity concentrations which follow Normal distributions (numerical experiments E1 to E7)[a].

	Entry parameters		Results from the linear regression and the CF-CS chronology					
	s_A	s_w	SAR ($g \cdot cm^{-2} y^{-1}$)	A_0 ($Bq \cdot kg^{-1}$)	Pearson's R^2	D-W[b]	ΔT_m (y)	ΔT_{max} (y)
E1	0.02	0.02	0.201 ± 0.001	99.6 ± 0.7	0.9995	2.17	0.14	0.34
E2	0.02	0.2	0.192 ± 0.001	100.5 ± 1.0	0.9991	1.21*	0.6	2.5
E3	0.2	0.02	0.206 ± 0.009	94 ± 7	0.9470	2.06	1.3	2.7
E4	0.2	0.2	0.197 ± 0.008	95 ± 7	0.9528	2.12	1.4	3.2
E5	0.3	0.3	0.183 ± 0.012	93 ± 11	0.8981	2.08	1.9	4.4
E6	0.2↑	0.2	0.158 ± 0.001	136 ± 3	0.9976	0.35*	10.9	21.7
E7	0.2	0.3↑	0.194 ± 0.009	114 ± 9	0.9488	1.90	5.7	10.5

ΔT_m is the mean value of the absolute deviations of CF-CS ages from the synthetic ones, and ΔT_{max} is the maximum value for such absolute deviations.
↑ This symbol indicates that the corresponding typified Normal distributions instead of being randomly ordered have been sorted with decreasing values downcore, in such a way that they simulate a continuous trend of increase with time of the associated magnitude. In all the cases Pearson's R^2 has $p < 0.0000$.
Annex A5, in ESM provides an excel file for reproducing these tests.

[a] The tests use synthetic cores of 30 slices of 1 cm thick, a realistic bulk density profile with early compaction, and the random entry of SARs and initial activity concentrations with mean values of 0.20 $g \cdot cm^{-2} y^{-1}$ and 100 $Bq \cdot kg^{-1}$, respectively, estimated by Eq. (1) from two sets of numbers following typified Normal distributions and randomly ordered. Each test defines particular values of s_A and s_w, builds de synthetic chronology and the LN[A(m)] plot, and then applies a linear fit for estimating SAR and the initial activity concentration.

[b] Durbin-Watson statistic; the asterisk indicates possible serial correlation.

assumption is needed for establishing a chronology (see Abril 2015; 2019). Alternatives for this fourth assumption are: iv-a) $^{210}Pb_{exc}$ fluxes onto the SWI are constant over time (CRS model; Appleby and Oldfield, 1978); iv-b) $^{210}Pb_{exc}$ initial activity concentrations are constant over time (CIC model; Goldberg, 1963); iv-c) $^{210}Pb_{exc}$ fluxes onto the SWI and sediment accumulation rates (SAR) are both constant over time (CF-CS model; Robbins, 1978); iv-d) $^{210}Pb_{exc}$ fluxes and SARs can independently vary over time, but imposing a particular (and non-physically justified) choice for a Fourier series expansion (SIT model; Carroll and Lerche, 2003; Abril, 2015); iv-e) varying $^{10}Pb_{exc}$ fluxes and SARs, but attaining a positive statistical correlation, as shown by Abril and Brunskill (2014) (TERESA model; Abril, 2016).

Varved sediments, for which an independent chronology is possible, enable the reconstruction of records of $^{210}Pb_{exc}$ palaeofluxes (F), SARs, and initial activity concentrations (A_0). They provide a unique chance for testing the different versions of the above fourth assumption. Abril and Brunskill (2014), based upon a wide and systematic survey on varved sediments from marine, riverine and lacustrine environments, found that $^{210}Pb_{exc}$ fluxes onto the SWI always varied over time while they statistically correlated with SAR. SAR and A_0 also varied with time, but they were uncorrelated. These authors explained their findings on the basis of a conceptual model of composite mass-flows carrying $^{210}Pb_{exc}$ inputs, both with intrinsic scatter.

The SIT model claims to contain the above statistical correlation among fluxes and SARs as a particular case. Nevertheless, it has been shown that this model lacks of a sound physical basis and, in particular, it makes a misuse of the Fourier series expansions (Abril, 2015). Consequently it will not be further considered in this work.

It could be thought that the temporal variability of F, SAR and A_0 automatically discards the application of the CRS, CIC and CF-CS models. Nevertheless, an analysis of the properties of model-errors has shown that the CRS chronologies can be acceptable even for varying rates of supply positively correlated with SAR, when such variations are randomly distributed in time around a mean value (Abril, 2019). This result can be extended to the CF-CS and CIC models, as shown in this paper. This kind of random variability in fluxes is expected to occur in relatively unperturbed and low-energetic aquatic environments, and it would be linked to short-term climatic variability. Thus, the many application cases of these models where their chronologies have been validated against independent chronostratigraphic markers are not in contradiction with the empirical evidence of widespread conditions of varying rates of supply.

Natural random variability in environmental conditions may be interrupted by some episodic events (heavy storms, surges, floods, etc.). In high-energy sedimentary systems, such as some estuarine and coastal areas, local sedimentary conditions may vary over time because the dynamic of sand-bars, the silting and diverting of water channels, etc. Anthropogenic impacts can alter the flows of matter and $^{210}Pb_{exc}$ activities reaching the aquatic sedimentary systems with gradual (e.g., deforestation and other changes in land use) or drastic and permanent changes (e.g., waterworks). Thus, it is possible to distinguish different situations where the temporal variability in fluxes has not a pure random character: i) changes in environmental conditions lead to a stepped shift on the mean value of F, over which a random variability is superposed (referred hereafter as stepped fluxes); ii) changes in environmental conditions lead to a continuous trend of increase/decrease in F; iii) episodic events with abnormal high or low fluxes; iv) any combination of the previous cases. In these situations one cannot expect a good performance of the CF-CS, CIC and CRS models, at least under their standard formulations.

Two questions then arise: i) how to detect non-random variability in F from the basic dataset the researcher can handle for the radiometric dating; ii) the selection of a suitable ^{210}Pb-based model for generating reliable chronologies in these cases.

Episodic events can be identified in the log-plot of the $^{210}Pb_{exc}$ profile as points with abnormal excursions out of the trend-line. These singularities act as influencing points, but they can be discarded in the application of CF-CS and CIC models to get reasonable proxies to the chronology. The mathematics of the CRS model captures the mean value of fluxes and tends to keep localized the effect of such singularities. For severe cases, a possible treatment is the truncation of the profile (e.g., see Arnaud et al., 2002; Abril et al., 2018). Thus, this paper will focus in the study of stepped and/or continuous trends of change in F, and TERESA model will play a relevant role for this goal.

TERESA uses the paradigm on fluxes and SARs found by Abril and Brunskill (2014). The starting point is the generation of frequency distributions of initial activity concentrations and SARs, which then are conveniently sorted downcore to fit the measured $^{210}Pb_{exc}$ profile. The first version of the model handles Normal distributions. Its applications till present are scarce, but they comprise synthetic cores, varved sediments and some cores from dynamical sedimentary systems in a harbour and estuaries (Abril, 2016; Botwe et al., 2017; Klubi et al., 2017). Nevertheless, the use of Normal distributions may not be appropriate enough for facing problems with steeped changes in fluxes and/or with sharp trends of continuous change. This paper will present a new version of the TERESA model working with multimodal distributions of initial activity concentrations and SARs.

Although they have been always present in the scientific literature,

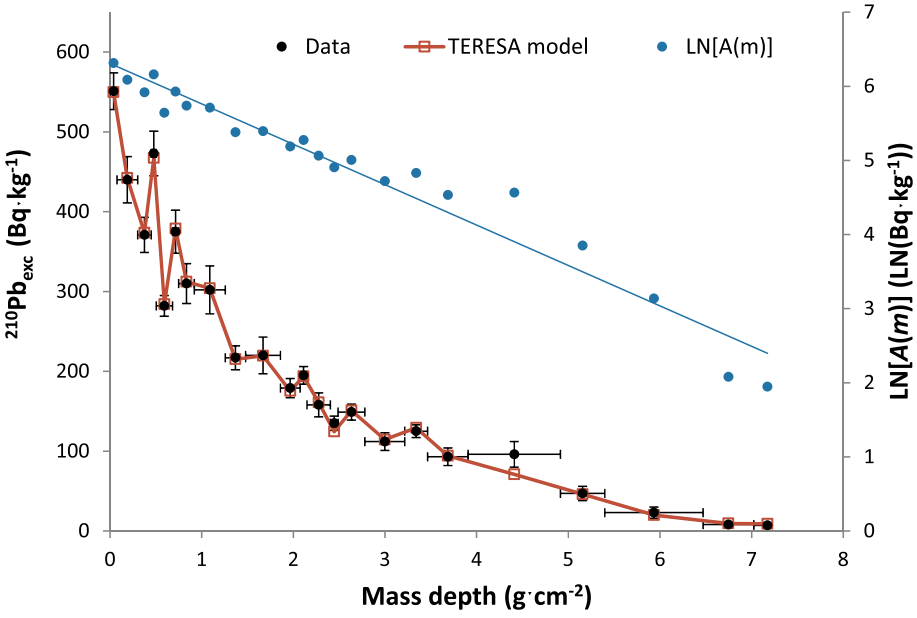

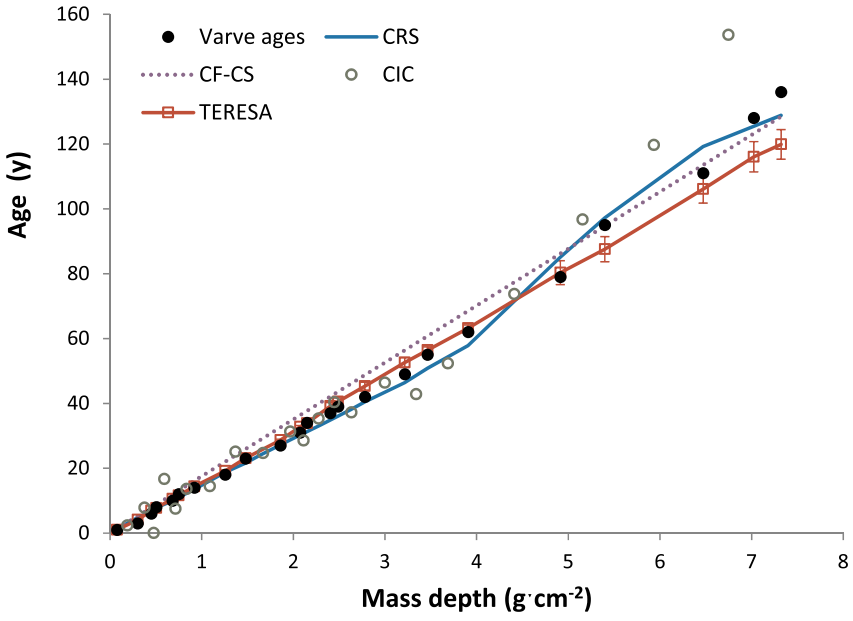

Fig. 1. Core C1: data and chronologies. First panel: $^{210}Pb_{exc}$ versus mass depth profile for core C1 (Pettaquamscutt River, data from Lima et al., 2005; Table A6-1, Annex A6, ESM). Vertical bars correspond to the associated uncertainties, while the horizontal ones define the mass depth interval of each sediment slice (also plotted in log-scale in the secondary axis). The best fit from TERESA model is plotted as points at the centre of each slice interval (continuous red line is only for guiding-eyes). The second panel plots the varve chronology and the ones generated by the CF-CS, CIC, CRS and TERESA models. For the sake of clarity propagated errors are depicted only for TERESA ages (error-bars).

in recent years there has been an increasing interest in studying high-energy and/or anthropogenically impacted sedimentary systems, where a non-random variability in $^{210}Pb_{exc}$ fluxes is expected to occur. They still represent one of the most challenging open questions in the radiometric dating of recent sediments. This work faces it with a sound methodology for identifying varying $^{210}Pb_{exc}$ fluxes, and with the combined use of the piecewise versions of CF-CS, CIC, CRS and TERESA models. The performance of the models will be tested against synthetic cores and real case studies with varve sediments for which independent chronologies are available. Present results also can serve for improving the reliability of other routinely applications, and they provide an updated perspective on the proper interpretation of model-outputs.

2. Materials and methods

2.1. Classical radiometric dating models

The primary object the researcher can handle after coring, sectioning and radiometric analyses, is the mass activity of $^{210}Pb_{exc}$ for each sediment slice, denoted hereafter as $A(m)$, with m being a mass-depth scale (mass depths are more meaningful than true depths because they remain invariant under natural compaction and the shortening during coring and storage). This dataset can be complemented with some independent chronostratigraphic marks, typically (but not only) the ^{137}Cs peaks.

A review of the CIC, CF-CS and CRS models can be seen, among others, in Sánchez-Cabeza and Ruíz-Fernández (2012). The work by Appleby (1998) provides a review of the CRS model, its problems and solutions. The associated techniques for using a piecewise CRS model

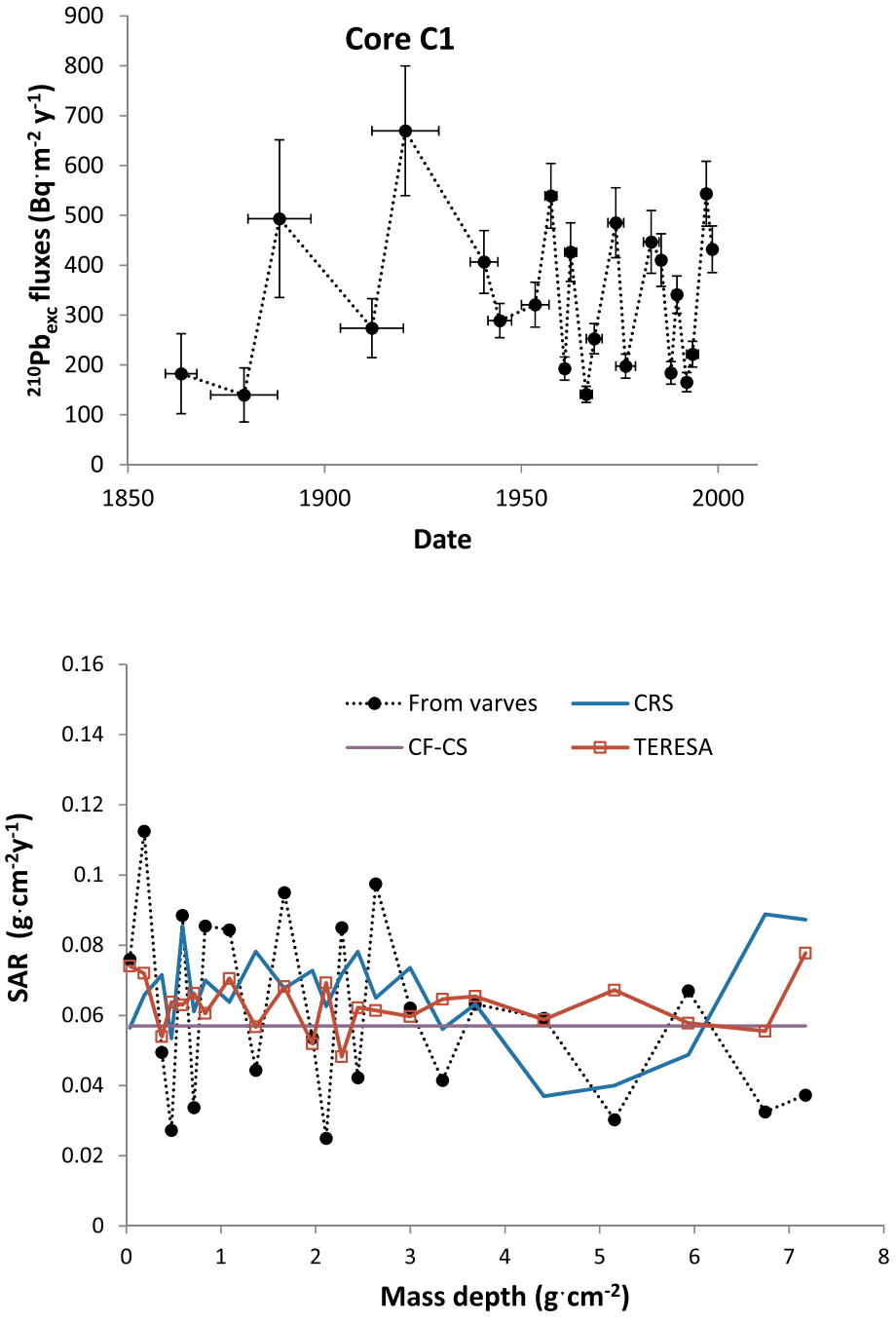

Fig. 2. Core C1: Palaeofluxes and SARs. First panel: Historical records of $^{210}Pb_{exc}$ palaeofluxes for core C1 (Pettaquamscutt River), as reconstructed from the varve chronology. Second panel: SAR from varves and from the CF-CS, CRS and TERESA models for core C1, as a function of mass depth.

can be found in the above work, and in Appleby (2001).

It is worth distinguishing between propagated-errors (from the uncertainties associated to direct measurements and the computations involved in the model) and model-errors (differences between model predictions and the true values, arising from a partial or null accomplishment of the model assumptions). A study of the properties of the CRS model-errors is presented in Abril (2019). Here we will adopt the notation used in this last reference, where the methodology for a piecewise application of the CF-CS model with up to three transects is also presented.

The Bayesian formulation of the CRS model (Aquino-López et al., 2018) will not be used here since it relays on the same set of model-assumptions. It is worth mentioning that this new formalism overcomes one of the major limitations of the classical CRS model, namely the need of handling an accurate estimation of the total $^{210}Pb_{exc}$ inventory.

2.2. *Identifying non-random temporal variability in $^{210}Pb_{exc}$ fluxes*

Changes in the mean value of F can be detected in cases where the ^{137}Cs time-marks (or other chronostratigraphic markers) allow estimating the equivalent constant $^{210}Pb_{exc}$ fluxes pre and post-dating a known reference date (Appleby, 2001; Abril, 2019). Alternatively, the new paradigm (Abril and Brunskill, 2014) allows tracking some long-term changes in F, which appear as jump and/or slope discontinuities in the logarithmic plot of $^{210}Pb_{exc}$ versus mass depth, LN[$A(m)$] (Abril, 2019). The above two methods can separately fail in some cases, but their simultaneous failure seems to have a low probability of

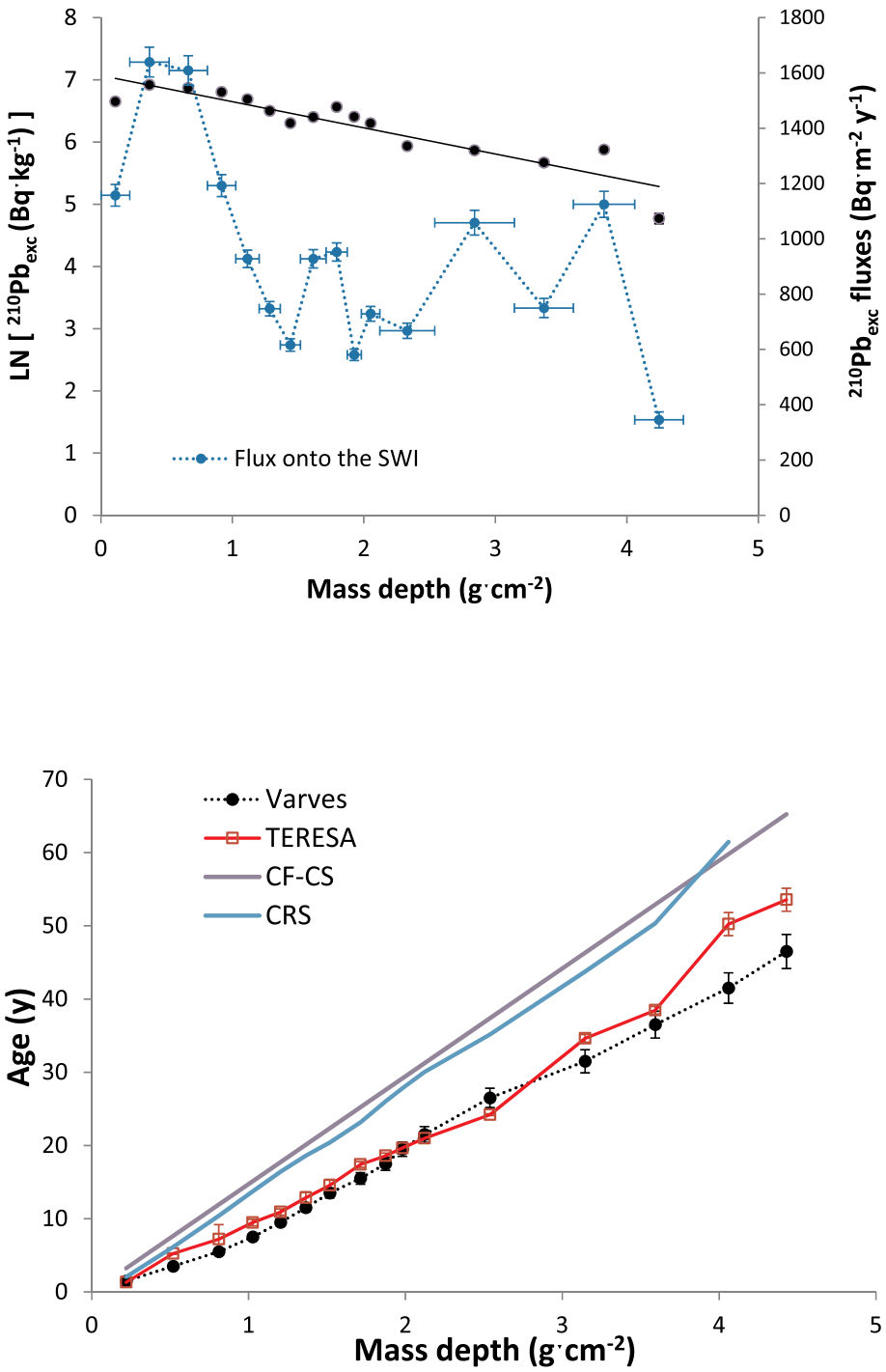

Fig. 3. Core C2: data, palaeofluxes and chronologies. First panel: LN[$A(m)$] plot and historical records of $^{210}Pb_{exc}$ palaeofluxes for core C2 (Santa Barbara Basin, data from Koide et al., 1973; Table A7-1, in Annex A7, ESM). Second panel: ages from varves and the chronologies generated by the CF-CS, CRS and TERESA models. For the sake of clarity propagated errors are depicted only for TERESA ages (error-bars).

occurrence.

Those cases with continuous trends of change in F are particularly challenging since they may not appear associated to discontinuities in the LN[$A(m)$] plot. In some cases, but not always, poor Pearson's correlation coefficients and/or positive Durbin-Watson tests can alert on non-random variability in F (Abril, 2019). In absence of independent time marks allowing estimating equivalent constant fluxes pre and post-dating the reference date, the situation may remain unidentified. In this work the TERESA model will be used for providing further insights.

2.3. TERESA model

The fundamentals of TERESA (Time Estimates from Random Entries of Sediments and Activities) model and its validation against synthetic cores and real data from varved sediments can be found in the work by Abril (2016). For the sake of completeness of the present work, a brief summary is presented in what follows.

The model stands on the set of assumptions i) to iii) (see the Introduction Section), and iv) $^{210}Pb_{exc}$ fluxes are governed by 'horizontal inputs', and thus there is a statistical correlation among fluxes and SARs

Table 2
Clusters analysis for the sediment core C3 (Portage Lake).

Parameters (from fit)		Sedimentary conditions			
Transect 1 ($N_1 = 6$)					
$-s_1$	0.2155 ± 0.035	$Ao_{,1}$	488 ± 12		
b_1	6.191 ± 0.025	w_1	0.144	±	0.023
Pearson's r, (p)	−0.951 ($p = 0.0035$)	F_1	700	±	110
m_1 discontinuity	1.25				
D-W	2.3				
Transect 2 ($N_2 = 6$)					
$-s_2$	0.370 ± 0.057	$Ao_{,2}$	418	±	32
b_2	5.766 ± 0.062	w_2	0.083	±	0.013
Pearson's r, (p)	−0.955 ($p = 0.003$)	F_2	350	±	60
D-W	3.2				
Global fit ($N = 12$)					
$-s$	0.386 ± 0.023	Ao	530 ± 21		
b	6.278 ± 0.039	w	0.081 ± 0.005		
Pearson's r, (p)	−0.982 ($p = 0.0000$)	F	430 ± 30		
D-W	2.1				

In the Ln[$A(m)$] plot (Fig. 4), $A(m)$ is given in Bq·kg^{-1} and m in g·cm^{-2}. $A_{o,i}$ and w_i (i = 1,2 –it refers to transects or clusters) have units of Bq·kg^{-1} and g·cm^{-2}y^{-1}, respectively, and F_i are given in Bq·m^{-2}y^{-1}; s_i are slopes, and b_i the independent terms in the linear fit. Values and errors in $A_{o,i}$ for i > 1have been estimated from Ln[$A(m')$] plots with a translation to the origin ($m' = m$-m_1 for $i = 2$). For the global fit a single cluster of data has been considered.

(Abril and Brunskill, 2014).

Natural variability in weather and other environmental conditions promote variability in the mass flows reaching the SWI, this is, in SAR (denoted as w). Such variability can be described by a continuous probability distribution, approached in the first version of the model by a Normal distribution. The above variability is also reflected in the relative contribution of particulate matter reaching the SWI from different erosional sites (catchment area and/or shallower unstable sedimentary deposits) and then on the average content of $^{210}Pb_{exc}$ they previously have accumulated and/or uptake on their transit. Empirical evidence shows that this variability in A_0 (also approached by a Normal distribution by TERESA) is uncorrelated with SAR (Abril and Brunskill, 2014).

The assumption of ideal deposition relates the fluxes with the above two magnitudes: $F = A_0\ w$. Then the positive statistical correlation between F and w automatically arises from the combination of the independent variability in A_0 and w. Thus, the $^{210}Pb_{exc}$ versus mass depth profile is the result of random combinations of A_0 and w values, and of the radioactive decay.

For a sediment core which has been sectioned into N slices of mass thickness Δm_i, (i = 1,2, … N), each one has an associated age interval, ΔT_i, a mean SAR value $w_i = \Delta m_i/\Delta T_i$, and an initial activity concentration $A_{0,i}$ (the one encountered for the sediment slice at the SWI). TERESA model operates with SARs and initial activities which for the slice i adopt the values (w_i, $A_{0,i}$), both varying along the core, but closely following Normal distributions around their respective arithmetic mean values, $\overline{w}$ and $\overline{A}_0$, with standard deviations σ_w and σ_A, respectively, being s_w and s_A their typified values (standard deviations divided by the mean values).

Provided a first estimation for $\overline{w}$, $\overline{A}_0$, σ_w and σ_A, the model generates independent random distributions for w_i and $A_{0,i}$. A practical way for achieving this is to generate two sets of N values, $z_{1,i}$ and $z_{2,i}$, following Normal typified distributions (this is, with mean value 0 and standard deviation 1.0). The numbers within the series $z_{1,i}$, and a $z_{2,i}$ must be randomly ordered, and maintained during all the routine calculations. This is not a trivial task, but there are some software tools, and a practical procedure is described in Abril (2016). Annex A1, in electronic supplementary material (ESM), provides a library with examples of $z_{1,i}$ and $z_{2,i}$ distributions for N ranging from 5 up to 50. The pairs ($A_{o,i}$, w_i) are then generated as follows:

$$A_{0,i} = \overline{A}_0\,(1 + s_A z_{1,i})$$
$$w_i = \overline{w}(1 + s_w z_{2,i}) \qquad (1)$$

A numerical code solves their best arrangement downcore to fit the experimental $A(m)$ profile. Thus, if the pair of index $i = k$ was been selected for the first sediment slice, of known mass thickness Δm_1, its age interval will be $\Delta T_1 = \Delta m_1/w_k$. Then, the expected (theoretical) averaged value of the $^{210}Pb_{exc}$ specific activity in this layer, $A_{th,1}$, can be estimated from the involved hypothesis and the radioactive-decay:

$$A_{th,1} = A_{0,k}\frac{1 - \exp(-\lambda\Delta T_1)}{\lambda\Delta T_1} \qquad (2)$$

The best choice for the pair k is the one which minimizes the absolute difference between $A_{Th,1}$ and the known value of the $^{210}Pb_{exc}$ mass activity concentration in the first sediment slice, A_1. For the second slice the previous value of ΔT_1 accumulates for applying radioactive decay. This way the code is generating the solutions for the chronological line and for the histories of SAR and fluxes. There are different ways for programming the sorting algorithm. Two methods (labelled A and B) are described in Abril (2016). Method A is the simplest one, and uses the same arrangement in all the iterations for the pairs ($z_{1,i}$, $z_{2,i}$), while Method B allows testing the use of each $z_{1,i}$ value when combined with all the possible $z_{2,j}$ values. Annex A2 (in ESM) provides an example of numerical code using method A, with its associated input and output files.

As the above result depends on the first estimation of $\overline{w}$, $\overline{A}_0$, s_w and s_A, the model applies a mapping technique by iterating the whole process for each parameter varying over a wide range (typically $2{\cdot}10^4$ iterations). The error function, Q^2, measures the overall quality of the fit for each individual run of the model:

$$Q^2 = \sum_{i=1}^{N}\frac{(A_{th,i} - A_i)^2}{\sigma_i^2}\ ;\ \chi^2 = Q^2\Big/f \qquad (3)$$

where here A_i and σ_i are, respectively, the measured value and the analytical error of the activity concentration at the slice with index i; $A_{th,i}$ is the corresponding value estimated by the model, and f is the number of degrees of freedom. Parametric maps of the χ-function serve to find out the best solution. These regions of the χ and Q^2 functions are further explored along the parametric lines for localizing the relative minimum with higher precision and for quantifying the fitting errors through the curvature of the parametric lines (Bevington and Robinson, 2003). Alternatively, the model output can be better constrained by independent time markers, when available, by introducing the concept of an "objective function" (Abril, 2016). Finally, propagated uncertainties can be estimated following standardized procedures.

For the first estimation of $\overline{w}$, $\overline{A}_0$, s_w and s_A, one can apply the CF-CS model and ascribing typical values of 35% and 20% for s_w and s_A, respectively. The mapping technique can explore a range up to 100% around the stated values, and they can be reset at any time. Annex A3 provides examples of codes for mapping χ. The output can be handled with graphical software, as the tools from MATLAB.

It is worth noting that TERESA does not need the total inventory, but measurements must be continuous over the sequence of sediment slices – otherwise, interpolations are needed. Also, and as with all the models, propagated uncertainties do not account for model-errors (in this case, the used Normal distributions are only a proxy to the real ones, but not an exact copy).

2.4. Multimodal TERESA

Normal distributions for A_0 and w are not appropriate enough for dating cores under steeped changes in fluxes and/or sharp trends of increase/decrease.

It is worth noting that when in the above described methodology we use very large values for s_w (or s_A) then w_i (or $A_{o,i}$) can take negative values in some sediment slices (Eq. (1)). This can be solved in the code by stating their minimum values, what in practice modifies the original Normal distributions (now approaching a Log-Normal). This method has

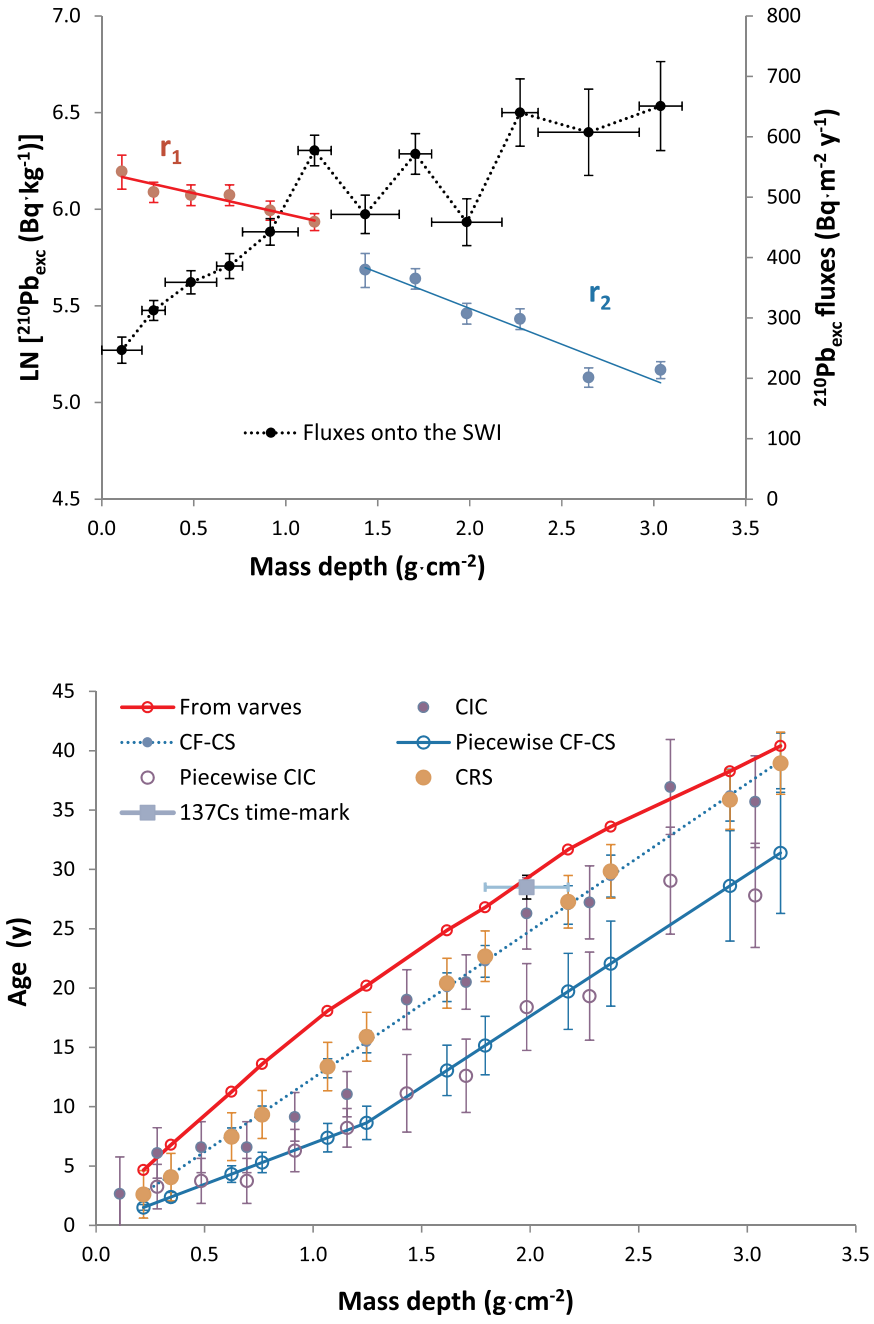

Fig. 4. Core C3: data, palaeofluxes and chronologies. First panel: LN[$A(m)$] plot with two transects (r_1 and r_2), and the historical records of $^{210}Pb_{exc}$ palaeofluxes for core C3 (Portage Lake, data from Kerfoot and Robbins, 1999). Second panel: Chronologies for core C3 from varves and classical models, including the piecewise versions of CF-CS and CIC. The ^{137}Cs time mark for 1963 is also depicted.

shown good performance in dynamic sedimentary systems from harbours and estuaries with very large variability in SARs (Botwe et al., 2017; Klubi et al., 2017). The use of Log-Normal distributions was already explored in Abril (2016) without noticeable advantages in the particular cases studied in that work.

Multimodal distributions will be studied here. Let us consider a sediment core with N slices and for which the LN[$A(m)$] plot shows two discontinuities defining three clusters of data, or regions with different mean values of A_0 and w, containing N_1, N_2 and N_3 data, respectively ($N = N_1+N_2+N_3$). Then, instead of two sets of N values, $z_{1,i}$ and $z_{2,i}$, following Normal typified distributions, we will generate 3×2 sets of $z_{1,i}$ and $z_{2,i}$ with lengths of data N_1, N_2 and N_3. Then we need ascribing first-estimate values of $\overline{w}$, $\overline{A}_0$, s_w and s_A for the three clusters (a good choice can be the values provided by a piecewise CF-CS model). Then the code will merge the three Normal distributions into a single and composite one (without any assignation to regions within the core) and proceed with the sorting algorithm as in the previous subsection. The error function Q^2 measures the overall quality of the fit. Now it is possible to run again the code by slightly modifying each entry parameter to minimize Q^2, what is achievable in a manageable number of iterations. This procedure will be referred as Fast Multimodal TERESA (FM-TERESA). Obviously, the described methodology can be adapted to any number of clusters. FM-TERESA can use the computed Q^2 for estimating the fitting errors in parameters. Annex A4, in ESM, provides an example

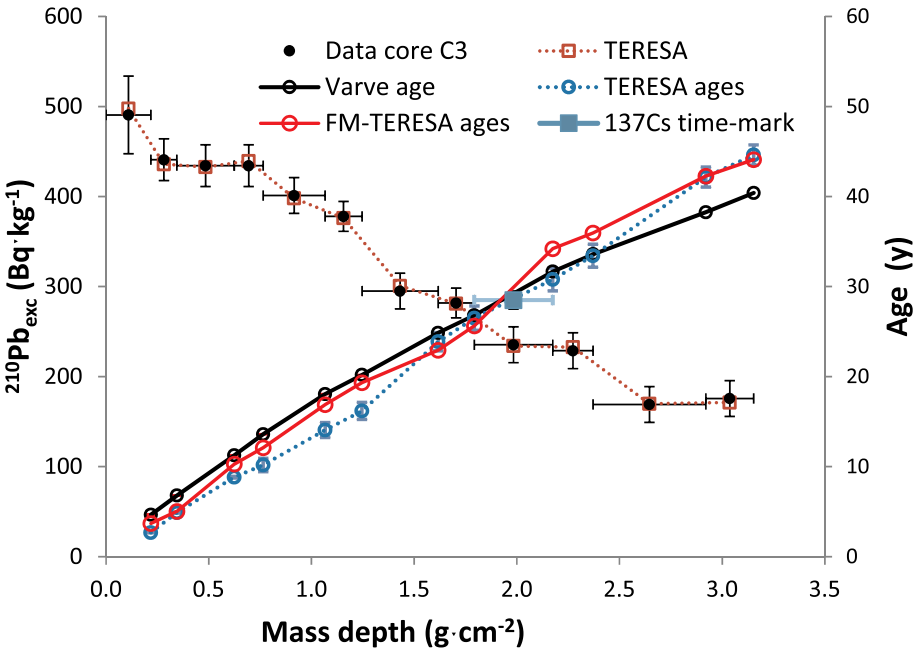

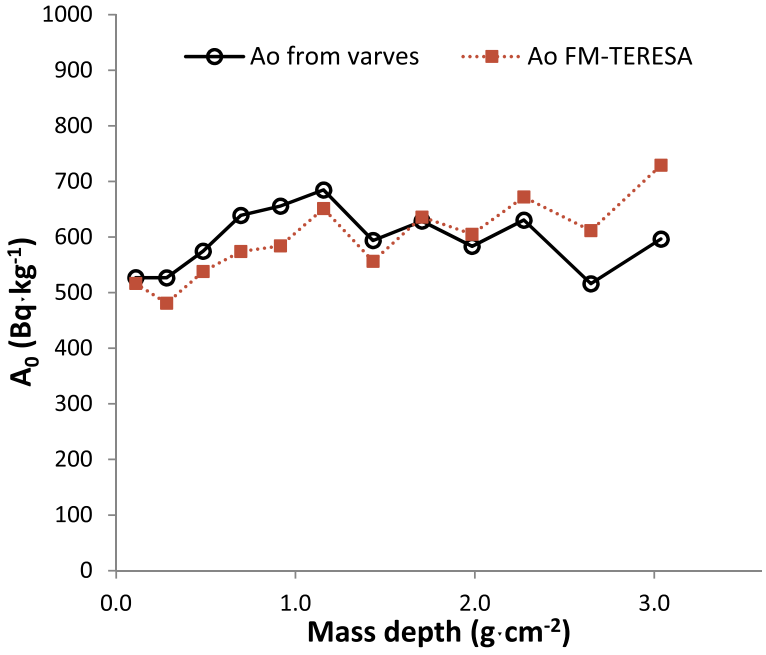

Fig. 5. Core C3: TERESA model. First panel: $^{210}Pb_{exc}$ versus mass depth profile for core C3. Vertical bars correspond to the associated uncertainties, while the horizontal ones define the mass depth interval of each sediment slice. The best fit from TERESA model is plotted as points at the centre of each slice interval (the dashed red line is only for guiding-eyes). In the secondary axis, the chronologies for core C3 from varves, TERESA, FM-TERESA and the ^{137}Cs time mark. Second panel: comparisons among initial activity concentrations (from varves) and the computed values by FM-TERESA model, as a function of mass depth.

of code for solving FM-TERESA.

Alternatively, TERESA can be sequentially applied by regions. As the model does not need the total inventory, it is possible selecting a first region with N_1 data (according to the clusters analysis, or any user-defined region), and proceed with the mapping technique, eventually supported by reference dates within the transect. The output of the model includes the estimation of the age at the bottom of the studied sediment region, $T_{f,1}$. Then a second region, containing N_2 slices, can be treated as a separated problem for TERESA, after a translation of the origin of coordinates ($m' = m\text{-}m_{f,1}$). The solution for the chronology for this second region must be corrected by adding $T_{f,1}$ and the initial activity concentrations (and fluxes) corrected by the factor $e^{\lambda T_{f,1}}$. The procedure can be repeated for additional regions. As for each region the model handles different Normal distributions (which here are not merged into a single one), as a whole it is a Multimodal-TERESA (M-TERESA).

2.5. *Core data and statistical analyses*

For testing the performance of all the models, this work uses sediment core data from published scientific works (references are provided in each particular case) for which a varve chronology is available and, when possible, supported by additional and independent chronostratigraphic marks. This is the basic dataset the researcher can handle, and the only one considered here, since our goals are methodological instead of in-deep studies for each core. Nevertheless, it is worth noting that

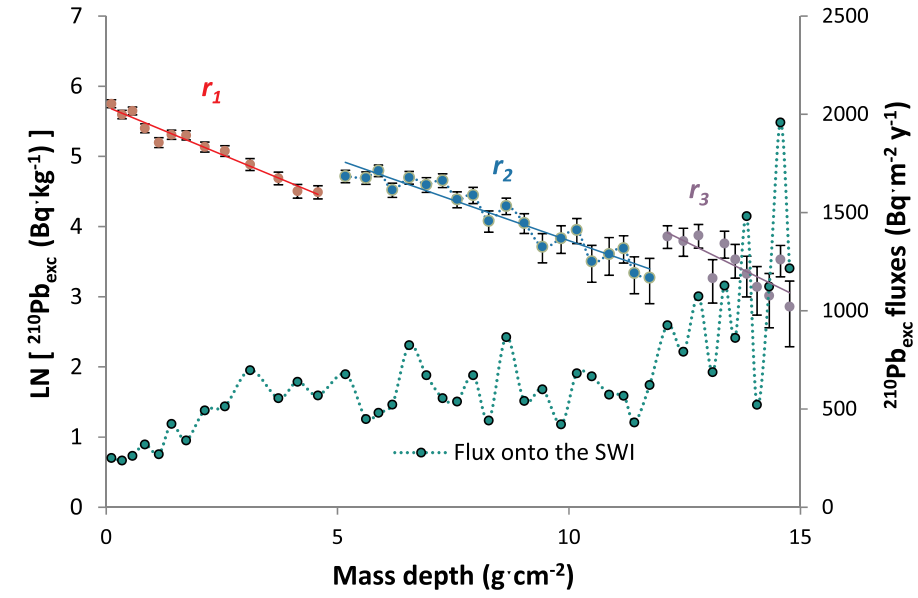

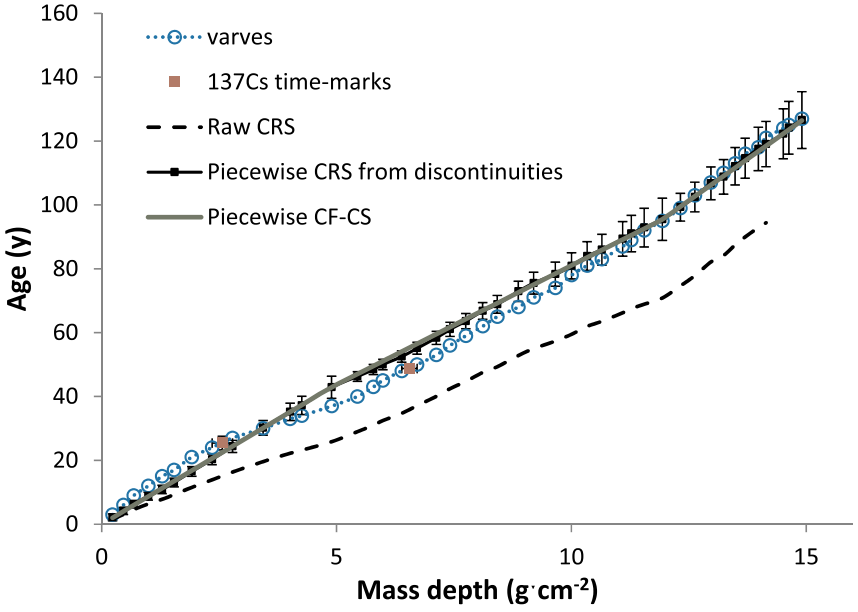

Fig. 6. Core C4: data, palaeofluxes and chronologies. First panel: LN[$A(m)$] plot with three transects (r_1, r_2 and r_3), and the historical records of $^{210}Pb_{exc}$ palaeofluxes for core C4 (Lake Zabinskie, data from Tylmann et al., 2016). A clusters analysis is reported in Table 3. Second panel: Chronologies for core C4 from varves, raw CRS and the piecewise versions of CF-CS and CRS (built with data from Table 3). The ^{137}Cs time marks for 1963 and 1986 are also depicted. For the sake of clarity only propagated errors are depicted for the piecewise CRS chronology.

other physical magnitudes, such as bulk density, LOI and mass concentrations of other natural radionuclides, can provide valuable insights which contribute to a more holistic analysis of the studied sedimentary system (e.g., Abril et al., 2018).

Reconstructions of palaeofluxes onto the SWI are reported following the methodology described in Abril and Brunskill (2014). This information will not be used as input data for models, but it will be helpful for understanding their functioning.

Synthetic cores will be used for testing the performance of CF-CS and CIC models under varying SARs and initial activity concentrations. They have been generated following the methodology described in Abril (2016), which involves realistic bulk density profiles and independent variability in SAR and A_0.

The statistical software package Statgraphics Centurion XVI has been used for linear regression analysis and for the estimation of the Durbin-Watson statistic.

3. Results and discussion

3.1. CF-CS, CIC and CRS models under varying $^{210}Pb_{exc}$ fluxes

It has been shown from analytical solutions and numerical simulations that for $^{210}Pb_{exc}$ fluxes onto the SWI with periodic-harmonic or random fluctuations around a baseline value, positive and negative deviations of the CRS chronology tend to cancel out (Abril, 2019). Thus, under these conditions the CRS-chronologies provide reasonable proxies to the true ones. The above reference also proves that CRS chronologies fail for continuous trends of increase/decrease in fluxes. The same applies for CF-CS and CIC model, as shown with the set of numerical experiments summarized in Table 1.

The numerical tests use synthetic cores of 30 slices of 1 cm thick each, a realistic bulk density profile with early compaction, and random SARs and A_0 with arithmetic mean values of 0.20 $g \cdot cm^{-2} y^{-1}$ and 100 $Bq \cdot kg^{-1}$, respectively. These particular settings do not limit the

Table 3
Clusters analysis for the sediment core C4 (Lake Zabinskie).

Parameters (from fit)		Sedimentary conditions			
Transect 1 ($N_1 = 13$)					
$-s_1$	0.273 ± 0.016	$Ao_{,1}$	301 ± 12		
b_1	5.71 ± 0.04	w_1	0.114 ± 0.007		
Pearson's r, (p)	-0.981 ($p = 0.0000$)	F_1	343 ± 25		
m_1 discontinuity	4.89				
D-W	1.68				
Transect 2 (N2 = 20)					
$-s_2$	0.232 ± 0.017	$Ao_{,2}$	550 ± 60		
b_2	4.98 ± 0.07	w_2	0.134	±	0.010
Pearson 's r, (p)	-0.956 ($p = 0.0000$)	F_2	740	±	90
m_2 discontinuity	11.94				
D-W	2.11				
Transect 3 (N3 = 11)					
$-s_3$	0.32 ± 0.08	$Ao_{,3}$	1040 ± 220		
b_3	3.98 ± 0.15	w_3	0.096 ± 0.025		
Pearson's r, (p)	-0.790 ($p = 0.0038$)	F_3	1000 ± 300		
D-W	2.95				

In the Ln[$A(m)$] plot (Fig. 6), $A(m)$ is given in Bq·kg^{-1} and m in g·cm^{-2}. $A_{o,i}$ and w_i (i = 1,2,3 –it refers to transects or clusters) have units of Bq·kg^{-1} and g·cm^{-2}y^{-1}, respectively, and F_i are given in Bq·m^{-2}y^{-1}; s_i are slopes, and b_i the independent terms in the linear fit. Values and errors in $A_{o,i}$ for i > 1have been estimated from Ln[$A(m')$] plots with a translation to the origin ($m' = m\text{-}m_1$ for $i = 2$; $m' = m\text{-}m_2$ for $i = 3$).

conclusions from present results. The pairs (w_i, $A_{0,i}$) are estimated by Eq.1 after stating s_w and s_A, and by using two sets of numbers following typified Normal distributions and randomly ordered. From the w_i values and the known mass thickness, the synthetic chronology arises, what allows generating the synthetic $A(m)$ profile. This is the primary object for stablishing a chronology and the application of CF-CS model follows with a linear fit to the LN[$A(m)$] plot, which provides the values for model-SAR and A_0. The goodness of the so derived CF-CS chronologies is reported through the mean value of the absolute deviations of CF-CS ages from the synthetic ones, ΔT_m, and the maximum value for such absolute deviations, ΔT_{max}. Annex A5, in ESM provides an excel file for reproducing these tests.

Table 1 shows that in all the cases where the variability in $A_{o,i}$ and w_i is randomly distributed in the time-line, the CF-CS model gives a good proxy to the synthetic chronology, being the variability in $A_{0,i}$ the major source of inaccuracy. When the typified Normal distribution used for generating $A_{o,i}$ is sorted with decreasing values downcore, one can simulate a continuous trend of increase in the initial activity concentration with time. This produces the catastrophic failure of the CF-CS model, with a wrong estimation of the mean SAR value, and then with a chronological line which diverges from the synthetic one. The model partially fails (depending on the case and on the final use of data) when the continuous trend of increase is introduced in SAR. In this case the mean SAR value is properly captured, but the synthetic chronology is a curve-line with noticeably distances from the CF-CS chronology, as shown in Figures in Annex A-5.

It is worth noting that the subjacent pattern of increasing SAR or A_0 (and then increasing fluxes) cannot be unambiguously detected from the LN[$A(m)$] plot. In all the cases the linear fit provides high R^2 values with $p < 0.0000$. As seen in Table 1, the Durbin-Watson statistic produces some false positives and fails to detect some true alerts.

When an independent chronostratigraphic mark is available it is possible estimating the equivalent constant $^{210}Pb_{exc}$ fluxes pre and post-dating the reference date. Their values should be similar when the variability is randomly distributed in time, but they may significantly differ under continuous trends of change. Thus, if in experiment E7 the synthetic age of ~56 y at the bottom of slice $i = 20$ is used as a known independent reference date, the equivalent constant $^{210}Pb_{exc}$ fluxes pre and post-dating such a mark are, respectively, 178 and 236 Bq·m^{-2}y^{-1}. The first computation requires estimating (by the reference-SAR method) the missing part of the inventory (as in the cases with incomplete recoveries). The assignation of analytical uncertainties to the synthetic profile is somehow arbitrary. With 10% of relative uncertainties in $A(m)$ the above figures are significantly different, alerting then on non-random variability in $^{210}Pb_{exc}$ fluxes. A similar test applied to E6 also detects non-random variability in fluxes. This test can avoid reporting wrong CF-CS and CRS chronologies, but leaves unsolved the dating problem.

A critical issue in the application of the CIC model to noisy $A(m)$ profiles is how to select the value for the initial activity concentration. In the above experiments the CIC chronologies can be built from the fitted value of A_0 (i.e., the ordinate in origin in the CF-CS model). The CIC ages show a random noise, with typical age reversals, but they follow the trend-line of the CF-CS chronology (see Annex A5). The trend-line defined by the cloud of CIC-ages is the physically meaningful chronology provided by this model. So, the above results also apply to the CIC model. Nevertheless, it is worth noting that if by some means the researcher could select as initial activity concentration the synthetic value, then the cloud of CIC ages would follow the synthetic chronology in the case of experiment E7, but the CIC-chronology also catastrophically fails in experiment E6.

The case of stepped changes in fluxes can be recognized by jump and/or slope discontinuities in the LN[$A(m)$] plot, which define several clusters or transects (Abril, 2019). By extension of previous results, some clusters with good linear regressions may hide continuous trends of change in fluxes. Thus, the use of reference dates, any available independent information, and/or the insights provided by a FM-TERESA model can be helpful to prevent misuses of the piecewise CF-CS, CIC and CRS models, as shown in the application cases below.

3.2. *Application case C1 (random variability in fluxes)*

Core C1 is a varved sediment sampled in April 1999 in the Pettaquamscutt River basin (Rhode Island, Northeast USA) at 41°30′N, 71°26′W and 19.5 m depth (data from Lima et al., 2005). Varves were defined by biogenic and clastic layers. Table A6-1(in Annex A6, ESM) reports raw data with the $^{210}Pb_{exc}$ profile and the varve chronology. The 1963 time mark from a ^{137}Cs peak was also available. Figure A6-1 (Annex A6, ESM) shows the statistical correlation which holds among palaeofluxes and SARs, both reconstructed by using the varve chronology. The histograms for the initial activity concentrations and SARs are shown in Fig. A6-2 (Annex A6, ESM). They are compatible with Normal distributions, although A_0 fits better a Log-Normal.

The linear regression for the LN[$A(m)$] plot (Fig. 1) has $R^2 = 0.951$ with $p < 0.0000$. Data can be described by a single cluster, although with noise at the deepest sediment slices, which have a coarser resolution. At the present state of the art, there are no quantitative criteria for splitting the above cluster of data, so it is a matter of the researcher's decision. This point will be considered some further. The ^{137}Cs peak (Table A6-1) can be ascribed to the maximum atmospheric fallout of 1963. The equivalent constant $^{210}Pb_{exc}$ fluxes pre and post-dating such a reference date are, respectively, 335 ± 19 and 308 ± 8 Bq·m^{-2}y^{-1}. For the first computation the missing part of the inventory due to its incomplete recovery has been estimated by the reference-SAR method -by using the global exponential fit to $A(m)$, and it represents less than 2% of the measured portion of the inventory. As both fluxes are not statistically different at 95% confidence level (CL) the application of the CF-CS, CIC and CRS models cannot be discarded. The corresponding chronologies are shown in Fig. 1 (second panel), compared against the ages from varves and the chronology from TERESA model.

Here we applied the first version of TERESA model (Section 2.3) with method A. The mapping of the χ function (Eq. (3)) appears in Figure A6-3 (Annex A6, ESM). The best fit to the observed $^{210}Pb_{exc}$ profile appears in Fig. 1 (first panel), and the fitting parameters, with their associated uncertainties are given in Table A6-2 (Annex A6, ESM). The sorting algorithm stars from top to down, what explains a poorer fit at the deepest sediment slices.

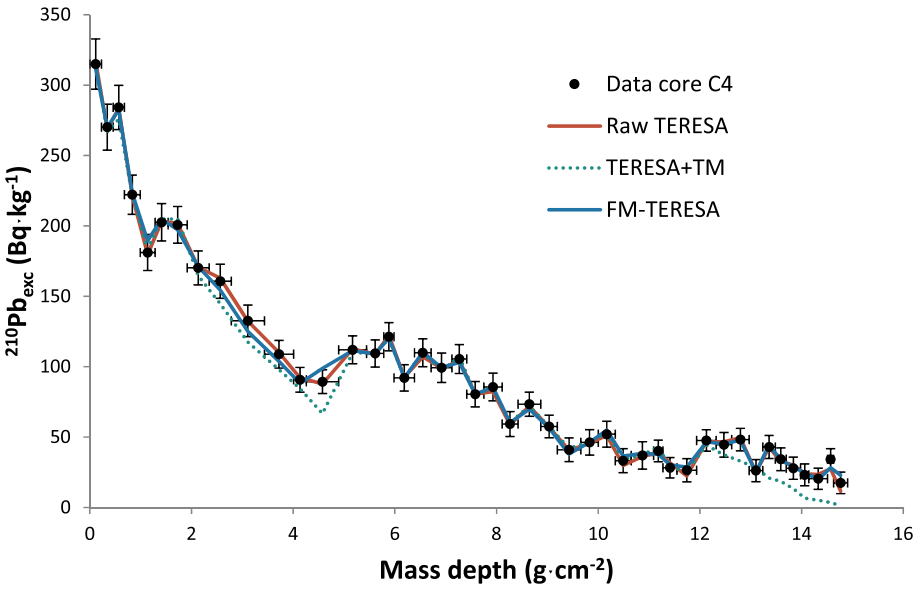

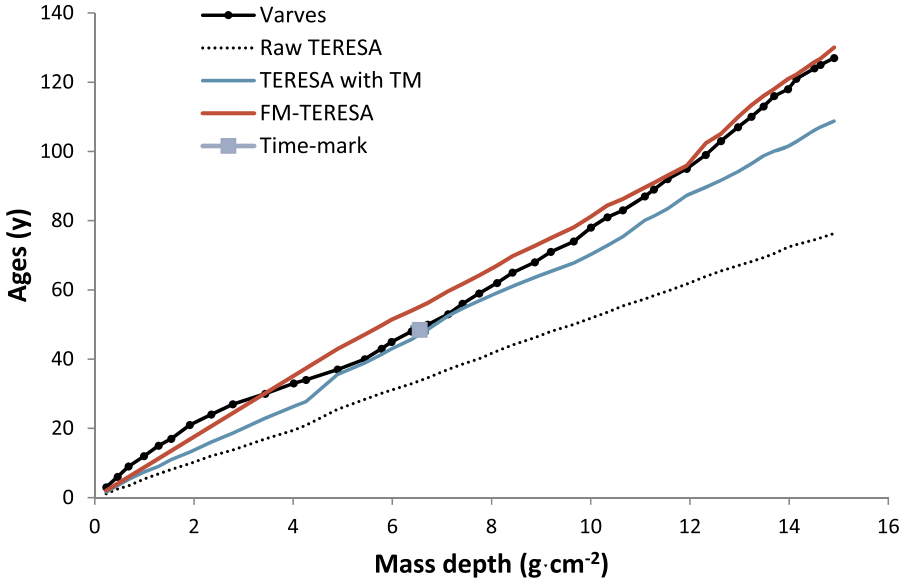

Fig. 7. Core C4: TERESA model. First panel: $^{210}Pb_{exc}$ versus mass depth profile for core C4. Vertical bars correspond to the associated uncertainties, while the horizontal ones define the mass depth interval of each sediment slice. The best fit from several versions of the TERESA model are plotted as points at the centre of each slice interval (colour lines are only for guiding-eyes). Second panel: Chronologies for core C4 from varves and from several versions of the TERESA model. The ^{137}Cs time mark for 1963 is also depicted. For the sake of clarity propagated errors have been omitted.

The four models show an overall good performance in producing a chronology close to the one from varves. This is what can be expected from a situation with random variability in fluxes. And this is essentially the case, as shown in Fig. 2, which plots the time records of palaeofluxes reconstructed from the varve chronology.

It is worth noting that none of the models is able to provide a high-accurate high-resolution SAR history (Fig. 2, second panel). Effectively, when a magnitude (F, A_0, w) is forced to be constant for the model construction, then its natural variability is compensated by spurious changes in the other magnitudes. TERESA allows a simultaneous variability in A_0 and w; but as it works with probability distributions which are only a proxy to the real ones, there is also some degree of mutual compensation in the model output. From Fig. 2, the only gross feature which can be reported is "random variability around a mean SAR value", and it is futile trying to associate any particular peak to eventual environmental changes. Also note that a random SAR is the only consistent result which can be expected from a raw CRS model (under the paradigm of fluxes statistically correlated with SARs).

All the chronologies provide a poor description for old ages. An alternative analysis which splits $A(m)$ into two clusters (by separating the last 5 points) can be seen in Abril (2019). It concluded that changes in initial activity concentrations and SARs mutually compensated, keeping the mean value for fluxes virtually constant.

In these cases with random variability in fluxes, when simultaneously confirmed by a reference date and the existence of a single cluster of data, the model choice is not too relevant, since all of them produce a similar output: a reasonable proxy to the true chronology and to the mean values of fluxes and SARs. Although simplicity is an advantage, the CRS and/or TERESA histories for SAR without trends of continuous changes over time can provide further self-consistency to the analysis.

3.3. *Application cases C2 and C3 (continuous trends of change in fluxes)*

3.3.1. *Core C2*

Core C2 was sampled in 1971 in Santa Barbara Basin, at geographical

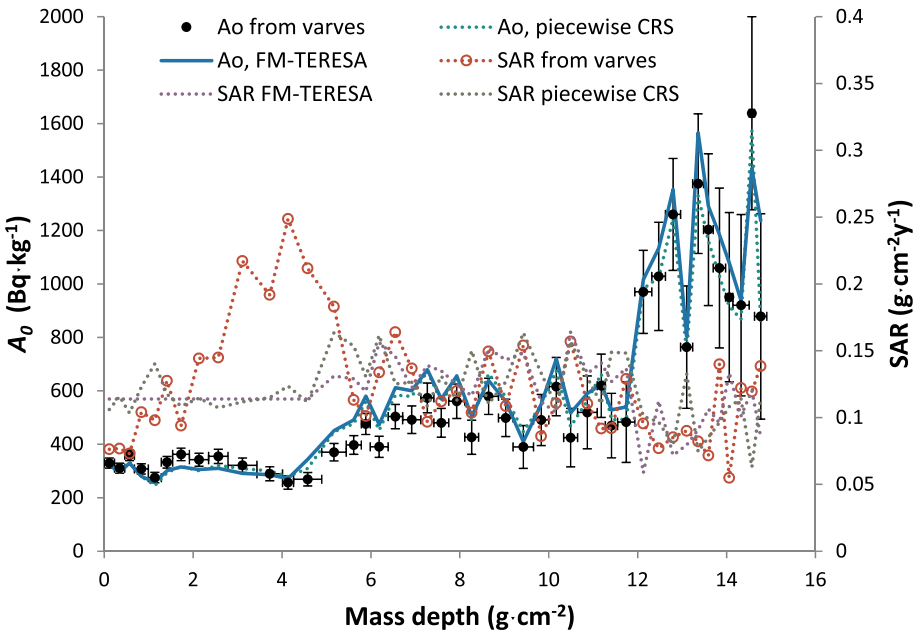

Fig. 8. Core C4: A_0 and SARs. Initial activity concentrations and SARs for core C4 as a function of mass depth. Data estimated from the varve chronology and from FM-TERESA and piecewise CRS models. Vertical bars in A_0 correspond to the associated uncertainties, while the horizontal ones define the mass depth interval of each sediment slice.

coordinates 34°14.0′N, 120°01.5′W and 575 m water depth. It is a varved sediment with annual designations based on a direct correlation of sediment thickness and rainfall for the past 100 yr (data from Koide et al., 1972, 1973). Raw data are reported in Table A7-1 (Annex A7, ESM). The reconstructed $^{210}Pb_{exc}$ palaeofluxes (Fig. 3) show random variations from 1930 to 1960, followed by a continuous trend of increase that peaked around 1970, shortly before the coring. In this case the increase in fluxes is mostly contributed by an increase in SAR (see Table A7-1).

The LN[$A(m)$] plot (Fig. 3) defines a single cluster of data with good linear regression ($R^2 = 0.838$, $p < 0.0000$; D-W = 1.86, $p = 0.28$). The application of the CF-CS, CIC and CRS models fail with too old ages diverging from the varve chronology (Fig. 3). TERESA model, with method A, gives a reasonable proxy to the varve chronology (Fig. 3, and more details in Abril, 2016).

In this case the clusters analysis does not alert from varying fluxes, and the ^{137}Cs time mark was not available for this core. Nevertheless, and for the sake of completeness in arguments, one could use the varve-age of 1963 as a reference date to estimate the pre and post-dating constant equivalent $^{210}Pb_{exc}$ fluxes, resulting of 662 ± 24 and 1460 ± 30 Bq·m^{-2}y^{-1}, respectively. These last figures certainly alert from varying fluxes, although nothing can be done with the CF-CS, CIC and CRS models, and a piecewise version of this last by using the above reference date also fails (see Abril, 2016).

In core C2 SARs and A_0 (from varves) can be approached by Normal distributions, and fluxes statistically correlated with SAR (Figs. A7-1 and A7-2, in Annex A7, ESM). Thus, the conditions for the application of TERESA model are meet, and although with poor statistics (N = 16), TERESA is able to capture an arrangement of fluxes with a trend-line of increase (slope 12 ± 6 Bq·m^{-2}y^{-2}, $p = 0.058$).

3.3.2. *Core C3*

Core C3 was sampled in the fall of 1991 in Portage Lake, at geographical coordinates 47°06′N, 80°30′W and 10–14 m water depth. It showed varve-like slime clay layers associated with mining discharges (original data from Kerfoot and Robbins, 1999). Raw data appear in Table A8-1 (Annex A8, ESM). For the present study data older than 1950 were excluded since they were affected by mining discharges.

The ^{137}Cs peak corresponding to 1963 was found at slice number 9 (Kerfoot et al., 1994). The pre and post-dating equivalent constant $^{210}Pb_{exc}$ fluxes take values of 480 ± 60 and 390 ± 9 Bq·m^{-2}y^{-1}, respectively. For estimating the first value, it was necessary correcting the total inventory by the reference-SAR method, and the correction represented about 40% of the measured portion of the $^{210}Pb_{exc}$ inventory. Statistically significant differences at 95% CL cannot be resolved for the above values of fluxes. A linear regression to the whole dataset (N = 12) shows good performance (Table 2). Thus, it could be though that the raw versions of CF-CS, CIC or CRS models would lead to good proxies to the true chronology. Nevertheless, this is not exactly the case and the three models produce ages younger than the ones from varves (Fig. 4). The failure compares with the situation of experiment E7 in Table 1 (see Figures in Annex 5), and attending only to the ^{137}Cs mark the chronology could be seen as acceptable, depending on the final use of data.

Alternatively, the researcher could distinguish two clusters of data in the LN[$A(m)$] plot (Fig. 4) with noticeably different slopes and both with good linear regressions (Table 2). The $^{210}Pb_{exc}$ flux onto the SWI takes statistically significant (95% CL) different values for the two transects (Table 2). A piecewise version of the above three models seems them to be justified. The chronologies from the piecewise CF-CS and CIC models are shown in Fig. 4. They use the SARs and initial activity concentrations from Table 2. The so obtained ages are even far below from the ^{137}Cs time mark and the varve ages. A piecewise CRS model is not discussed here because the needed correction for the missing part of the inventory is too high.

The reconstructed palaeofluxes are shown in Fig. 4, first panel. They show a continuous trend of decrease in the top sediment (recent ages), preceded by a period with random variability around a constant mean value. The continuous trend of decrease in fluxes is in this case contributed by a decrease in both, A_0 and SAR, but mostly by this last magnitude (SAR is reported in Table A8-1, and A_0 is plotted in Fig. 5). This continuous trend of change in fluxes is the reason for the failure of the previous models.

The clusters analysis, apart from the statistical tests, essentially consists in the application of a piecewise CF-CS model. Consequently, it fails there where the CF-CS model fails, this is, in those transects which

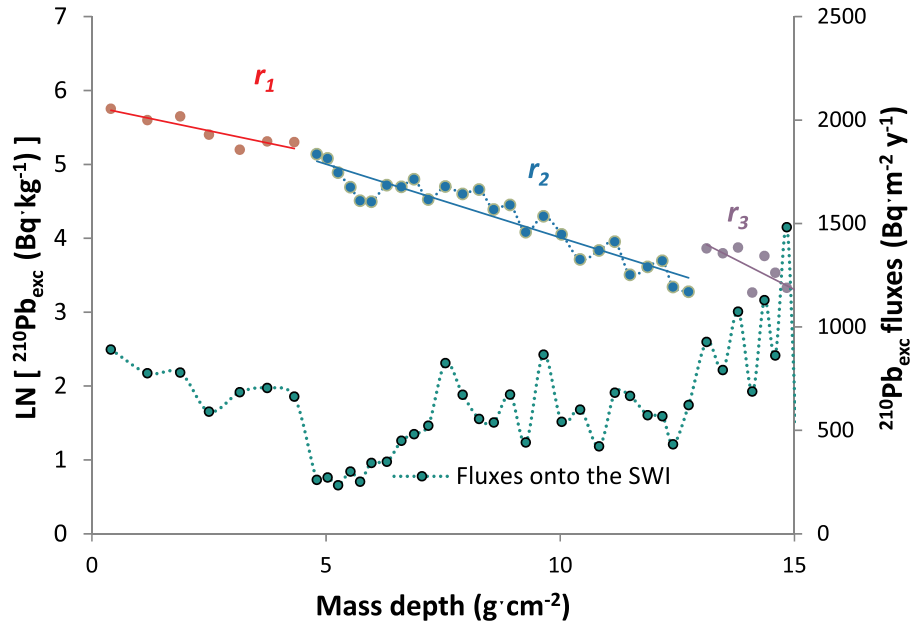

Fig. 9. Core C4B: data, palaeofluxes and chronologies. First panel: LN[$A(m)$] plot with three transects (r_1, r_2 and r_3), and the historical records of $^{210}Pb_{exc}$ palaeofluxes for core C4B (synthetic, from C4). A clusters analysis is reported in Table A10-1 (Annex A10, ESM). Second panel: Chronologies for core C4B from varves, the piecewise versions of CF-CS and CRS (built with data from Table A10-1), from FM-TERESA and for M-TERESA (three transects). For the sake of clarity propagated errors have been omitted.

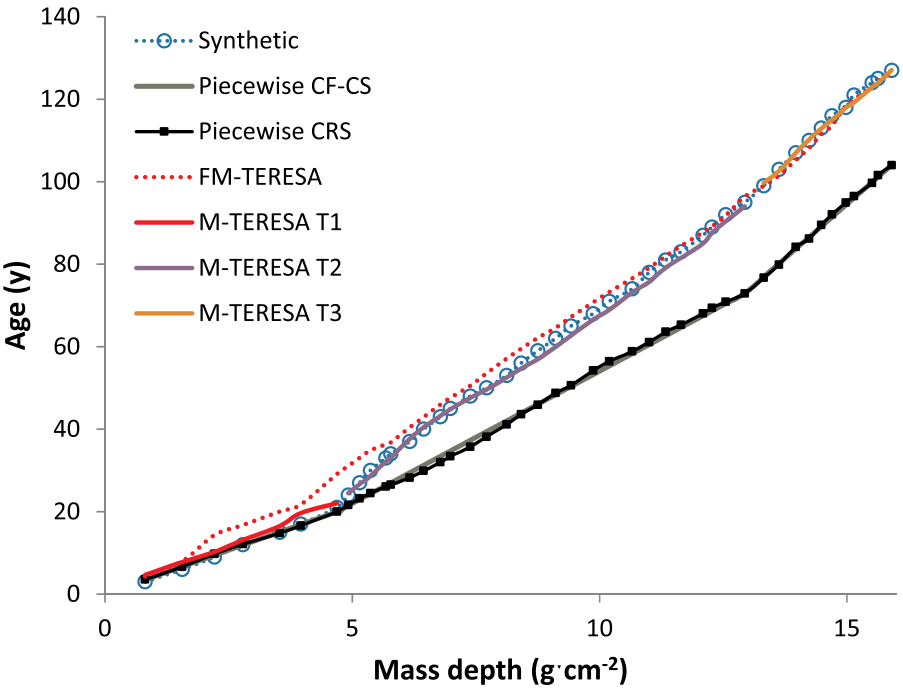

hide continuous trends of change in fluxes. In this case it leads to a wrong estimation of the $^{210}Pb_{exc}$ flux in the first transect (Table 2), since decreasing fluxes resulted in a flattening in the $A(m)$ profile (Fig. 5, first panel), which is interpreted by the CF-CS model as a scenario with high SAR.

As seem in Fig. A8-1 (Annex A8, ESM), the statistical correlation among $^{210}Pb_{exc}$ and SAR also holds for this core, and the variability in SAR and initial activity concentrations are compatible with Normal distributions (Fig. A8-2).

The application of TERESA model is able to produce a reasonable proxy to the varve chronology (Fig. 5, first panel), despite the poor statistic (N = 12) and the gross-description provided by the Normal distributions. The mapping of the χ function is presented in Fig. A8-3, and the fitting parameters with their associated uncertainties are reported in Table A8-2 (both in Annex A8, ESM).

The use of the FM-TERESA model is also illustrated with two transects (see fitting parameters in Table A8-2). Now the multimodal distributions slightly improve the chronology (Fig. 5; $\Delta T_{max} = 4.0$ y and $\Delta T_m = 1.9$ y), and FM-TERESA provides a gross description of the major features in the variability of A_0 (Fig. 5, second panel). It is worth noting

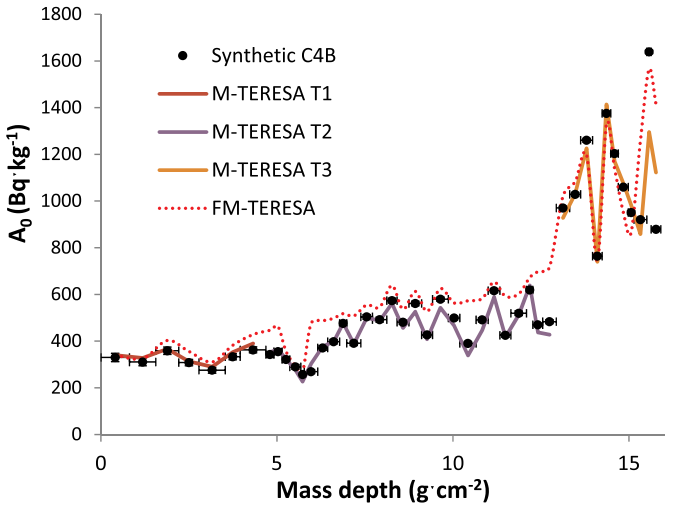

Fig. 10. Core C4B: A_0 by M-TERESA. Initial activity concentrations for core C4B as a function of mass depth (synthetic values and the ones estimated from FM-TERESA and M-TERESA with three transects).

that only this basic understanding is what can be expected from a model with a statistical basis but working with a very scarce dataset.

3.4. Application cases C4 and C4B (stepped fluxes with hidden continuous trends of change)

3.4.1. Core C4

Data for core C4 are available in the supplementary material from the work by Tylmann et al. (2016). The sediment core was collected in September 2011 in Lake Zabinskie at 54°07′54.50″ N; 21°59′01.1″ E and 44.4 m water depth. The core showed biogenic varves, and authors provided, among others, the ^{137}Cs time-marks for 1963 and 1986 (Chernobyl). The constant equivalent ^{210}Pb$_{exc}$ fluxes for the three transects defined by the above reference dates were (in the order of increasing ages): 319 ± 8, 568 ± 18 and 692 ± 28 Bq·m^{-2} y^{-1}. This reveals important changes in the mean value of fluxes. The Ln[$A(m)$] plot for this core (Fig. 6) shows three transects with two jump discontinuities. The interpretation of the fitting parameters (Table 3) reveals an increase in the mean value of the initial activity concentrations and fluxes after the two transitions.

Core C4 is a good example for non-random variability in ^{210}Pb$_{exc}$ fluxes confirmed by both, the reference dates and the clusters analysis. In absence of the varve chronology, this could be seen as a case of pure stepped changes in fluxes.

It is worth noting that a linear regression to the whole dataset also shows good performance ($r = -0.959$, $p = 0.0000$), but the raw version of the CF-CS, CIC and CRS models fail to fit the time marks, leading to ages much younger than those from varves (for the sake of clarity only the raw CRS chronology is plotted in Fig. 6). Again, the reason for such failure is the non-random temporal variability in ^{210}Pb$_{exc}$ fluxes.

The piecewise version of the CF-CS model provides a reasonable proxy to the reference dates, as shown in Tylmann et al. (2016) and in Fig. 6. The same is true for the CIC chronology (not shown) and for a piecewise CRS model working with the true ages of the discontinuities (Fig. 6). These reference ages have been estimated from the mass depth of the discontinuity and the mean SAR values for each transect (Table 3). A detailed discussion on the constraints in using the ^{137}Cs reference dates for a piecewise CRS model can be seen in Abril (2019). When compared against the varve chronology, the piecewise versions of the classical models provide an overall good agreement (e.g., for the piecewise CRS $\Delta T_{max} = 6.3$ y and $\Delta T_m = 2.3$ y).

In core C4 the reconstructed palaeofluxes largely varied with time (Fig. 6, panel 1). The paradigm for fluxes correlating with SARs is attained within each transect (Fig. A9-1, Annex A9, ESM). Also within each transect the frequency distributions for A_0 and SAR are compatible with Normal distributions, although the fit is poor. Concerning the whole core, A_0 does not fit a normal distribution ($p = 0.029$ for the Kolmogorov-Smirnov test), but it is compatible with a Log-Normal distribution (Fig. A9-2, Annex A9, ESM).

The performance of TERESA model for this core has been studied with the following approaches: i) raw TERESA; ii) TERESA with a time-mark; iii) FM-TERESA.

In this case raw-TERESA is able to produce a good fit to $A(m)$, with $\chi = 0.26$, but with an unacceptable chronology (Fig. 7) –the mapping of χ is reported in Fig. A9-3, and the fitting parameters in Table A9-1 (Annex A9, ESM). The failure can be detected from the known reference dates (when available, as in this case) and/or by the cluster analysis (Fig. 6 and Table 3), which alerts from large changes in A_0 that cannot be reasonably described by using Normal distributions.

The use of a reference date (in this case the 1963 peak in the ^{137}Cs profile) for constraining TERESA shows a better performance in chronologies, although its fit to $A(m)$ is poorer (Fig. 7, $\chi = 1.1$). The mapping of the objective function is reported in Fig. A9-4, with fitting parameters reported in Table A9-1 (Annex A9, ESM). This method ensures good performance of the chronology around the reference date, but discrepancies may be high at other regions because the limitations of monomodal distributions. This justifies the need of an improved version of TERESA model.

The FM-TERESA produces a good fit to the $A(m)$ profile ($\chi = 0.40$) and a good proxy to the varve chronology (Fig. 7; $\Delta T_{max} = 7.1$ y, $\Delta T_m = 3.5$ y). The fitting parameters are reported in Table A9-1 (Annex A9, ESM). The chronology is virtually identical to that produced by the piecewise versions of the CF-CS and CRS models (Fig. 6) and, as in these cases, the only inputs are from the ^{210}Pb$_{exc}$ data.

In transect 1 there is a clear trend of decreasing fluxes (Fig. 6), but this did not produce the global failure in the piecewise classical models, although their chronologies show regions with negative and positive deviations in transects 1 and 2, respectively. More properly, there are two pseudo-failures of the type of experiment E7 (Table 1, and Annex 5) but with opposite signs. Effectively, Fig. 8 shows the values for SARs and A_0 from the varve chronology as a function of mass depth, and it can be seen a noticeable peak in SAR around the transition between transects 1 and 2. Thus the decreasing fluxes in transect 1 are mostly governed by decreasing SARs, but the CF-CS model is able to capture its mean value, fitting the true chronology at its both ends, as in experiment E7. Transect 2 incorporates the effect of the pre-peak increase in SAR.

The piecewise CRS has been built on the basis of the CF-CS reference dates, so both produce similar chronologies. Thus, although the experiments in Section 3.1 have shown that continuous trends of change can produce the failure of classical models, in real complex cases there may coexist opposite trends of increase and decrease in the meaningful magnitudes, and the final effect on chronologies may depend on each particular situation. This last will be illustrated further below with core C4B.

Fig. 8 shows the values of SAR and A_0 computed by FM-TERESA and the piecewise CRS model, which are similar. They only capture the mean value of SAR in each transect, but both models can reproduce with reasonable detail the temporal changes in A_0. This gives a good chance for relating them with major historical environmental changes. Thus A_0 is better than SARs for tracking such changes. This is a novel result, since most of the studies till present have used the (spurious) variability in SAR.

3.4.2. Core C4B

Core C4B is a synthetic core built con the basis of C4, but changing its recent history of SAR and fluxes: i) SAR values from slices 1–7 have been exchanged with those from slices 8–14; ii) the new first two values have been changed to 0.27 and 0.25 g·cm^{-2}y^{-1} to keep a plateau with high SAR values in recent years; iii) the ages at the bottom of each slice and

the mass activity concentrations of $^{210}Pb_{exc}$ have been preserved from core C4; iv) the mass depth intervals and the paleofluxes have been consistently updated. The resulting $^{210}Pb_{exc}$ and SAR versus mass depth profiles are shown in Fig. A10-1 (Annex A10, ESM), while the LN[$A(m)$] plot is depicted in Fig. 9 along with the synthetic palaeofluxes.

The LN[$A(m)$] plot (Fig. 9) allows defining three transects with different lengths than in the case of core C4. Transect 1, including seven sediment slices, corresponds to the region of recent high SAR values (Fig. A10-1). Transect 2 includes 26 slices, and in its upper region there is a trend of decreasing fluxes (Fig. 9). The corresponding clusters analysis is reported in Table A10-1 (Annex A10, ESM). The piecewise CF-CS is able to capture the mean value of SAR in transect 1, but it overestimates its mean value in transect 2 leading to a failure of the chronology (Fig. 9). The same is true for the piecewise CRS model, since it has been built on the basis of the CF-CS reference dates.

In this case FM-TERESA produces a reasonably proxy for the chronology (Fig. 9), although with a poor description for recent ages. The application of M-TERESA with three transects gives much better estimates for the chronology (Fig. 9; $\Delta T_{max} = 2.65$ y, $\Delta T_m = 1.1$ y). The mapping of the χ function in the three transects can be seen in Fig. A10-2, and the piecewise fit to the $A(m)$ profile appears in Fig. A10-3 (both in Annex A10, ESM). Finally, the fitting parameters appears in Table A10-2. Again, M-TERESA is able to capture the temporal changes in A_0 (Fig. 10).

4. Conclusions

i) Empirical evidences from varved sediments show that natural sedimentary conditions are characterized by large temporal and independent variability in SAR and A_0. Although this contradicts the assumptions of the classical CF-CS, CIC and CRS models, they still are able to provide reasonable proxies for the chronologies when the above variability is randomly distributed in the timeline around a constant mean value (Sections 3.1 and 3.2). This type of variability is expected to occur in non-perturbed and low-energy aquatic environments.

ii) Non-random temporal variability in fluxes is expected to occur in anthropogenically impacted and/or high-energy aquatic environments. It makes to fail the above classical models. In real complex cases there may coexist opposite trends of changes and their final effect on the chronology will depend on each particular situation.

iii) The estimation of equivalent constant $^{210}Pb_{exc}$ fluxes pre and post-dating a known reference date and the clusters analysis of the LN[$A(m)$] plots are powerful tools for identifying non-random temporal variability in fluxes. A comprehensive inter-comparison of outputs from TERESA and the classical models can provide additional insights on the studied sedimentary conditions.

iv) Sediment cores with pure stepped changes in fluxes can be dated with the piecewise versions of the CF-CS, CIC and CRS models. In this last case the references dates must be those of the true discontinuities in fluxes.

v) Continuous trends of change in fluxes are not associated to discontinuities in the LN[$A(m)$] plot. In some cases they can be detected by the reference-date method. All the classical models, including their piecewise versions, fail to date these cases.

vi) TERESA and Multimodal TERESA have shown to be promising tools for dating sediments with stepped and continuous trends of change in fluxes. The last model can be applied under its FM version (merging several Normal distributions) or sequentially by transects (M-TERESA).

vii) The use of TERESA model relies on the suitability of multimodal distributions to mimic the real ones, and on the capability of the $A(m)$ profile to attract the true solution from a virtually infinite number of possibilities. While the first point can be subject to refinements, the second is still poorly understood, and a good fit (a low χ value) does not guarantee a reliable chronology. TERESA still needs to be supported by independent chronostratigraphic marks and by the holistic analysis of all the available meaningful information on the studied sedimentary system.

viii) Reporting propagated uncertainties in model-ages is scientifically consistent, but it must be taking in mind that there are also non-quantified model-errors.

ix) A reliable chronology does not guarantee a confident high-resolution high-accuracy SAR history. TERESA and the (piecewise) CRS models can provide reasonable proxies for the history of A_0. Thus, this magnitude is more suitable than SAR for tracking major historical environmental changes.

Declaration of competing interest

The author declares no conflicts of interest.

Acknowledgements

This research did not receive any specific grant from funding agencies in the public, commercial, or not-for-profit sectors.

References

Abril, J.M., 2003. A new theoretical treatment of compaction and the advective-diffusive processes in sediments. A reviewed basis for radiometric dating models. J. Paleolimnol. 30, 363–370.

Abril, J.M., 2015. Why would we use the Sediment Isotope Tomography (SIT) model to establish a ^{210}Pb-based chronology in recent-sediment cores? J. Environ. Radioact. 143, 40–46.

Abril, J.M., 2016. A ^{210}Pb-based chronological model for recent sediments with random entries of mass and activities: model development. J. Environ. Radioact. 151, 64–74.

Abril, J.M., 2019. Radiometric dating of recent sediments: on the performance of ^{210}Pb-based CRS chronologies under varying rates of supply. Quat. Geochronol. 51, 1–14.

Abril, J.M., Brunskill, G.J., 2014. Evidence that excess ^{210}Pb flux varies with sediment accumulation rate and implications for dating recent sediments. J. Paleolimnol. 52, 121–137.

Abril, J.M., Gharbi, F., 2012. Radiometric dating of recent sediments: beyond the boundary conditions. J. Paleolimnol. 48, 449–460.

Abril, J.M., San Miguel, E.G., Ruiz-Cánovas, C., Casas-Ruiz, M., Bolívar, J.P., 2018. From floodplain to aquatic sediments: radiogeochronological fingerprints in a sediment core from the mining impacted Sancho Reservoir (SW Spain). Sci. Total Environ. 631–632, 866–878. https://doi.org/10.1016/j.scitotenv.2018.03.114.

Appleby, P.G., 1998. Dating recent sediments by ^{210}Pb: problems and solutions. In: Illus, E. (Ed.), Dating of Sediments and Determination of Sedimentation Rate. STUK A-145, Finland, pp. 7–24.

Appleby, P.G., 2001. Chronostratigraphic techniques in recent sediments. In: Last, W.L., Smol, J.P. (Eds.), Tracking Environmental Change Using Lake Sediments. Basin Analysis, Coring, and Chronological Techniques. Developments in Paleoenvironmental Research. Kluwer, Dordrecht, pp. 171–203.

Appleby, P.G., Oldfield, F., 1978. The calculation of lead-210 dates assuming a constant rate of supply of unsupported ^{210}Pb to the sediment. Catena 5, 1–8.

Aquino-López, M.A., Blaauw, M., Christen, J.A., Sanderson, N.K., 2018. Bayesian analysis of ^{210}Pb dating. J. Agric. Biol. Environ. Stat. 23, 317–333.

Arnaud, F., Lignier, V., Revel, M., Desmet, M., Beck, C., Pourchet, M., Charlet, F., Trentesaux, A., Tribovillard, N., 2002. Flood and earthquake disturbance of ^{210}Pb geochronology (lake Anterne, NW Alps). Terra. Nova 14 (4), 225–232.

Bevington, P.A., Robinson, D.K., 2003. Data Reduction and Error Analysis for the Physical Sciences, third ed. McGraw-Hill, New York.

Botwe, B.O., Abril, J.M., Schirone, A., Barsanti, M., Delbono, I., Delfanti, R., Nyarko, E., Lens, P.N.L., 2017. Settling fluxes and sediment accumulation rates by the combined use of sediment traps and sediment cores in Tema Harbour (Ghana). Sci. Total Environ. 609, 1114–1125.

Carroll, J., Lerche, I., 2003. Sedimentary Processes: Quantification Using Radionuclides. Elsevier, Oxford.

Christensen, E.R., 1982. A model for radionuclides in sediments influenced by mixing and compaction. J. Geophys. Res. 87, 566–572.

Goldberg, E.D., 1963. Geochronology with Pb-210. In: Proceedings of a Symposium of Radioactive Dating. International Atomic Energy Agency, Vienna, pp. 121–131.

Kerfoot, W.C., Lauster, G., Robbins, J.A., 1994. Paleolimnological study of copper mining around Lake Superior: artificial varves from Portage Lake provide a high resolution record. Limnol. Oceanogr. 39 (3), 649–669.

Kerfoot, W.C., Robbins, J.A., 1999. Nearshore regions of Lake Superior: multi-element signatures of mining discharges and a test of Pb-210 deposition under conditions of variable sediment mass flux. J. Gt. Lakes Res. 25, 697–720.

Koide, M., Soutar, A., Goldberg, E.D., 1972. Marine geochronology with ^{210}Pb. Earth Planet. Sci. Lett. 14, 442–446.

Koide, M., Bruland, K., Goldberg, E.D., 1973. Th-228/Th-232 and Pb-210 geochronologies in marine and lake sediments. Geochem. Cosmochim. Acta 37, 1171–1187.

Klubi, E., Abril, J.M., Nyarko, E., Laissaoui, A., Benmansour, M., 2017. Radioecological assessment and radiometric dating of sediment cores from dynamic sedimentary systems of Pra and Volta estuaries (Ghana) along the Equatorial Atlantic. J. Environ. Radioact. 178–179, 116–126.

Lima, A.L., Hubeny, J.B., Reddy, C.M., King, J.W., Hughen, K.A., Eglinton, T.I., 2005. High resolution historical records from Pettaquamscutt River basin sediments: 1. ^{210}Pb and varve chronologies validate record of ^{137}Cs released by the Chernobyl accident. Geochem. Cosmochim. Acta 69, 1803–1812.

Mabit, L., Benmansour, M., Abril, J.M., Walling, D.E., Meusburger, K., Iurian, A.R., Bernard, C., Tarjan, S., Owens, P.N., Blake, W.H., Alewell, C., 2014. Fallout ^{210}Pb as a soil and sediment tracer in catchment sediment budget investigations: a review. Earth Sci. Rev. 138, 335–351.

Robbins, J.A., 1978. Geochemical and Geophysical applications of radioactive lead isotopes. In: Nriago, J.P. (Ed.), Biochemistry of Lead in the Environment. Elsevier, Amsterdam, pp. 285–393.

Robbins, J.A., Edgington, D.N., 1975. Determination of recent sedimentation rates in Lake Michigan using ^{210}Pb and ^{137}Cs. Geochem. Cosmochim. Acta 39, 285–304.

Sánchez-Cabeza, J.A., Ruíz-Fernández, A.C., 2012. ^{210}Pb sediment radiochronology: an integrated formulation and classification of dating models. Geochem. Cosmochim. Acta 82, 183–200.

Tylmann, W., Bonk, A., Goslar, T., Wulf, S., Grosjean, M., 2016. Calibrating ^{210}Pb dating results with varve chronology and independent chronostratigraphic markers: problems and implications. Quat. Geochronol. 32, 1–10.